Supplementary Information for

Structure-guided design fine-tunes pharmacokinetics, tolerability, and antitumor profile of multispecific frizzled antibodies

Swetha Raman, Melissa Beilschmidt, Minh To, Kevin Lin, Francine Lui, Yazen Jmeian, Mark Ng, Minerva Fernandez, Ying Fu, Keith Mascall, Alejandro Duque, Xiaowei Wang, Guohua Pan, Stephane Angers, Jason Moffat, Sachdev S. Sidhu, Jeanne Magram, Angus M. Sinclair, Johan Fransson, Jean-Philippe Julien

Johan Fransson; Jean-Philippe Julien

Email: jfransson@northernbiologics.com; jean-philippe.julien@sickkids.ca

This PDF file includes:

Supplementary Information Text

Materials and methods

Antibody generation

Multi-specific FZD blocking antibodies mAb F2.I, F7.B and F6 were obtained by previously-described phage display experiments (1). Antibody variants were generated by site-directed mutagenesis using a Quikchange II XL kit (Agilent) with oligonucleotide primers (IDT). Expression of the antibodies was performed using the Expi293 Expression System (Life Technologies) whereby cells were transiently transfected with the constructs and cultured for six days at 37°C. Purification of the antibodies was performed using recombinant Protein A Sepharose (GE healthcare) and dialyzed against 1x PBS, pH 7.4.

32D cell line generation

The IL-3 dependent mouse cell line 32D was maintained in RPMI 1640 medium supplemented with 15% FBS, 50 U/mL penicillin, 50 µg/mL streptomycin, 2 mM L-glutamine, and 2 ng/mL recombinant murine IL-3 (PeproTech). To obtain 32D cells expressing FZD1, 2, 4, 5, 7 or 8, 2 x 10^6 cells were transfected with 2 µg DNA from the V5-tagged FZD construct using a Nucleofector 4D device (Lonza) according to the manufacturer's protocol (SF cell-line, Lonza, program DN-100). Stable clones were selected with 4 µg/mL blasticidin (Gibco) and maintained in growth medium supplemented with 2 µg/mL blasticidin. Cells were sorted using the BD FACS Aria II Cell Sorter for high FZD expression, using 100 nM mAb F2.I (multi-specific FZD IgG). A goat anti-human Alexa488 mAb (Jackson Immunoresearch) was used for detection.

β-catenin stabilization assay

In order to assess β-catenin stabilized protein levels, 1x10^6 cells per well were plated in 96-well plates with or without IgGs in a total volume of 0.2 mL. Cells were treated with 1500 ng/mL rhWnt3a (R&D Systems) for 2 h, before being lysed in cell extraction buffer (Abcam) supplemented with a complete mini protease inhibitor cocktail (Roche) for 30 min at 4°C. Protein concentrations were determined using the Bradford Protein Quantification Assay Kit (Thermo Fisher) and β-catenin was quantified using a β-Catenin

ELISA Kit (Abcam), following the manufacturer's instructions. Each treatment was run with technical duplicates for a total of at least N=2.

HPAF-II proliferation assay

HPAF-II cells were purchased from American Type Culture Collection (ATCC® CRL-1997™). Cells were plated in 96-well plates at a density of 2500 cells per well in 75 µL of EMEM containing 10% FBS and Pen/Strep. Plates were incubated overnight at 37°C and 5% CO_2 to allow cells to adhere. Test agents were diluted in PBS and a 25 µL volume was added to the wells. LGK974 (1 µM; AdooQ Bioscience) was used as a positive control. After four days, media was removed and media containing new test agents were added and cells were further incubated for 2-3 days. Endpoint analysis was performed using CellTiter-Glo (Promega Corp.) following the manufacturer's instructions. Data were normalized to PBS and LGK974 controls. Experiments were run in technical duplicates, for a total of N=3.

Animal studies

Animal work was performed at either the University Health Network Animal Resources Centre according to the guidelines of the University of Toronto Animal Care Committee (UACC) under AUP# 5565.2 or at Charles River Discovery Services North Carolina, accredited by the Association for Assessment and Accreditation of Laboratory Animal Care International. Female nude mice (Crl:NU(NCr)-Foxn1nu) were purchased from Charles River (North Carolina). C57Bl/6 mice were purchased from The Jackson Laboratory (Bar Harbor, ME).

Exposure studies

Plasma samples were collected from whole blood by centrifugation at 1500xg for 15 min (4°C), and supernatant was collected and maintained at -80°C. Plasma samples were thawed on ice and experiments were run the same day. Total IgG4 protein concentrations were determined using the Human Therapeutic IgG4 ELISA Kit (Caymen Chemical) following the manufacturer's instructions. Standard curves were generated in kit assay buffer using 2-fold serial dilutions of the appropriate IgG for each treatment group. Data

generated was analyzed in Prism (GraphPad). Analysis was performed using the four-parameter variable slope logistic equation. Each sample was run in duplicate.

Histopathology

Small intestine (duodenum, jejunum, ileum) and colon tissues were collected from three animals per treatment, flushed and fixed overnight before being processed into paraffin blocks. Samples were sectioned at 5 μm thickness and stained with hematoxylin and eosin (H&E). Slides were then transferred to a board-certified veterinary pathologist for microscopic evaluation.

Construct design, protein expression and purification

The gene for the human FZD-CRD construct FZD1 (residues 104-233), FZD2 (residues 24-156), FZD4 (residues 42-179), FZD5 (residues 28-150), FZD7 (residues 42-179) and FZD8 (residues 29-151), containing a C-terminal HRV-3C protease cleavage site followed by a linker, a mVenus tag and a tandem His_{12x} tag was codon-optimized for expression in human cells (GeneArt) and cloned into the pHLsec vector (2, 3). Human FZD-CRD used in binding studies were transiently transfected and expressed in suspension HEK 293F cells and purified using Ni-NTA affinity chromatography. The protein was eluted with an increasing gradient of imidazole with a maximum concentration of 500 mM, in a buffer containing 20 mM Tris, pH 8.0, 500 mM NaCl and 5% (v/v) glycerol. This step was followed by gel filtration chromatography (Superdex 200 Increase, GE Healthcare) in 20 mM Tris pH 8.0 and 150 mM NaCl buffer. For structural studies the FZD-CRD were expressed in HEK 293S (Gnt $I^{-/-}$) cells and purified as described above. The purified samples were then treated with His-tagged HRV-3C protease (Life Technologies) and Endoglycosidase H (EndoH, New England Biolabs). The cleaved and deglycosylated sample was purified by a second round of Ni-NTA affinity and size exclusion chromatography.

Fabs were transiently expressed in HEK 293F cells and purified using KappaSelect affinity chromatography (GE Healthcare), followed by cation exchange chromatography (MonoS, GE Healthcare) and size exclusion chromatography (Superdex 200 Increase 10/300 GL, GE Healthcare). For mAb F7.B used in structural studies, the Fab was expressed in HEK 293S (Gnt $I^{-/-}$) cells, and an additional EndoH treatment was performed before ion-

exchange chromatography. For complex formation, purified Fabs and FZD-CRDs were mixed at a 1:2.5 molar ratio and incubated at room temperature for 30 min. The complex was purified using a Superdex 200 Increase 10/300 GL column (GE Healthcare) in 20 mM Tris, pH 8.0 and 150 mM NaCl.

Crystallization and structure determination of FZD-CRD-Fab complexes

Co-complexes were concentrated and set up for crystallization at concentrations of 6-8 mg/mL. Proteins were mixed with conditions from sparse matrix screens (JCSG Top96 and Mycrolytic MCSG) in a 1:1 ratio. The FZD5-F2.I complex crystallized in a condition containing 0.2 M magnesium formate and 20% (w/v) PEG 3350 and diffracted to a resolution of 1.8 Å. The FZD7-F7.B complex crystallized in a condition containing 0.1 M CAPS, pH 10.5, 20% (w/v) PEG 3350 and 0.2 M NaCl, and diffracted to a resolution of 2.1 Å. The FZD7-F6 complex crystallized in a condition containing 0.2 M Na_2HPO_4, 20% (w/v) PEG 3350 and diffracted to a resolution of 2.5 Å. Data for the FZD5-F2.I and FZD7-F7.B complexes were collected at the 08ID-1 beamline at the Canadian Light Source, and that for the FZD7-F6 complex was collected at the 23-ID-D beamline at the Argonne Photon Source. The data were processed and scaled using XDS (4). Structures were determined by molecular replacement using Phaser (5) with FZD4 (PDB ID: 5BPB) (2) or FZD8 (PDB ID: 4F0A) (6) and Fabs from our internal database as search models. Iterations of model building and refinement were performed using Coot (7) and phenix.refine (8). All software were accessed through SBGrid (9). Data collection and refinement statistics are reported in Table S1.

Capillary isoelectric focusing (cIEF)

cIEF was performed using a Maurice instrument and a cIEF Cartridge (Protein Simple, San Jose, CA). For sample preparation, 50 µg of sample was mixed with a solution containing 8 M urea, 3% Pharmalyte (pH 3-10; GE Healthcare), 0.35% methyl cellulose and pI markers (Protein Simple). The sample mixture was injected into the cartridge and focused by applying a potential of 1500 V for 1 min as the first focusing step and a potential of 3000 V for 5.5 min as the second focusing step. Data were analyzed using Maurice software (Protein Simple).

Hydrophobic Interaction Chromatography (HIC)

HIC was performed in an HPLC system (Agilent 1290 Infinity II LC). 15 µg of sample was injected in a TSKgel Ether-5PW column (Tosoh Bioscience). A 25 min linear gradient (0-100 % of Buffer B: 0.1 M sodium phosphate, pH 6.5) was performed at a flow rate 1 ml/min (Buffer A: 0.1 M sodium phosphate, 1.5 M ammonium sulfate, pH 6.5). Data was analyzed using the instrument software.

Binding and competition assay using biolayer interferometry (BLI)

To determine the binding kinetics for Fabs F2.I, F7.B, F6 and Fab variants against recombinant FZD CRDs, BLI experiments were performed on an Octet Red96 instrument (FortéBio) at 25°C. All proteins were diluted in 1X kinetics buffer (PBS, pH 7.4, 0.01 % (w/v) BSA, 0.002 % (v/v) Tween-20). 10 µg/mL of FZD-CRD-mVenus was immobilized on Ni-NTA sensors. Following a 60 s baseline step, the loaded biosensors were dipped into wells containing serial dilutions of Fab, to determine the rate of association. Sensors were then dipped back into kinetics buffer to monitor the dissociation rate. The curves were fitted to a 1:1 binding model and the kinetic parameters (k_{on} and k_{off}) and equilibrium dissociation constant (K_D) were evaluated using FortéBio's Data Analysis software 9.0. Each reported value represents the average of three independent experiments. For the tandem competition assay, FZD-CRD-mVenus was immobilized on Ni-NTA sensors at a concentration of 10 ug/mL. The FZD-CRD was allowed to interact with the first Fab, followed by a baseline step and then was dipped into the second Fab.

HPAF-II xenograft tumor model

Female Ath/nu mice were implanted with 4 X 10^6 HPAF-II pancreatic epithelial cells (ATCC® CRL-1997™) in 50% Matrigel into the flank. Once tumors reached an average of 123 mm^3 (five days after tumor cell injection), mice were divided into four groups, with no statistically significant differences in starting tumor volume between any groups. Mice were dosed i.p. with either Vehicle (PBS) control, mAb F2.Iv2 (30 mg/kg), mAb F6 (30 mg/kg) or mAb OMP-18R5 (30 mg/kg) twice per week. Tumor and weight measurements were taken twice per week. Study endpoint was determined once control tumors reached 15 mm in any dimension (29 days after tumor cell injection), or if any health issues were visible.

Reverse transcription and quantitative real-time PCR

HPAF-II tumors were collected from treated mice at study endpoint, and flash-frozen. Samples were homogenized using a liquid nitrogen-cooled mortar and pestle. RNA was extracted using TRIzol® Reagent (Thermo Fisher) in combination with the RNeasy Mini Kit (Qiagen), following the manufacturer's protocol for both. On-column gDNA removal was performed using the RNase-Free DNase Set (Qiagen). RNA was quantified using the NanoDrop One Spectrophotometer (Thermo Fisher), and 2 μg of RNA was used to make cDNA using the RT^2 First Strand Kit (Qiagen). Real-Time PCR was performed on the Bio-Rad CFX384™ Real-Time PCR Detection System, using RT^2 SYBR Green Fluor qPCR Mastermix (Qiagen) and the Human WNT Signaling Pathway RT^2 Profiler™ PCR Array (Qiagen). Cq values were calculated using the Bio-Rad CFX Manager 3.1 software. Relative gene expression was determined using the 2^-ΔΔCq calculation, where ΔCq is determined by subtracting the Cq of each sample from the geometric mean of five housekeeping genes (ACTB, B2M, GAPDH, HPRT and RPLP0). Samples were then normalized to the treatment control (ΔΔCq) by subtracting the average ΔCq from all control samples (i.e. PBS-treated mice) from the ΔCq of each individual sample. Expression fold-change was then determined using the calculation 2^-ΔΔCq.

Statistical analyses

Significance was determined using Student's t-tests or analysis of variance using GraphPad Prism 7.0 software; p-values are defined as: * <0.05 ** <0.01 *** <0.001 **** <0.0001.

A

IgG ID#	Binding to 32D-FZD Cells (EC_{50}, nM)						Inhibition of β catenin stabilization (IC_{50}, nM)					
	FZD1	FZD2	FZD4	FZD5	FZD7	FZD8	FZD1	FZD2	FZD4	FZD5	FZD7	FZD8
F2.I	2.6	2.9	2.7	2.0	2.5	1.0	1.0	1.7	0.6	1.7	1.0	0.1
F7.B	0.3	0.3	1.2	0.2	0.4	0.1	1.3	1.1	0.4	0.3	1.2	4.2
F6	1.5	1.3	> 300	0.8	1.0	0.5	6.2	0.9	> 300	4.2	1.0	0.8

B

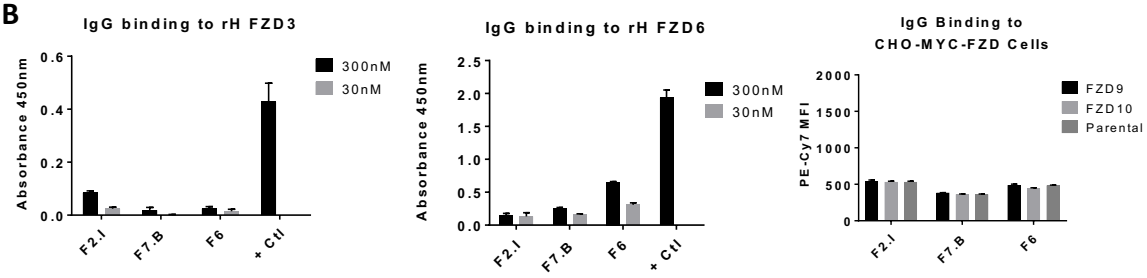

C

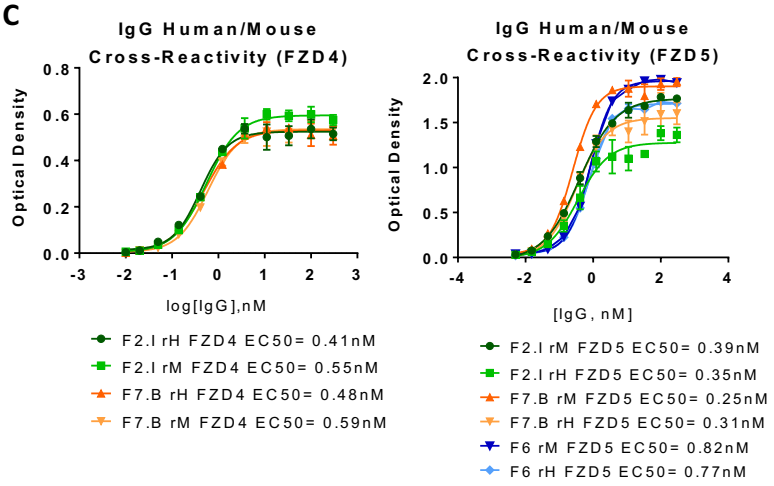

Figure S1: Cell-binding reactivity of mAbs. A) EC_{50} and IC_{50} values for mAbs F2.I, F7.B and F6 binding to, and inhibiting β-catenin stabilization in, 32D-FZD1, 2, 4, 5, 7 and 8 cells. B) IgG ELISA binding data for rFZD3 (far left panel), rFZD6 (middle panel), and IgG flow cytometry binding data to CHO-MYC-FZD9 and FZD10 (far right panel) showing lack of binding of mAbs F2.I, F7.B and F6 to FZD3, 6, 9, 10. C) Cross-reactivity of mAbs F2.I and F7.B to mouse FZD4 (left panel) and mAbs F2.I, F7.B and F6 to FZD5 (right panel).

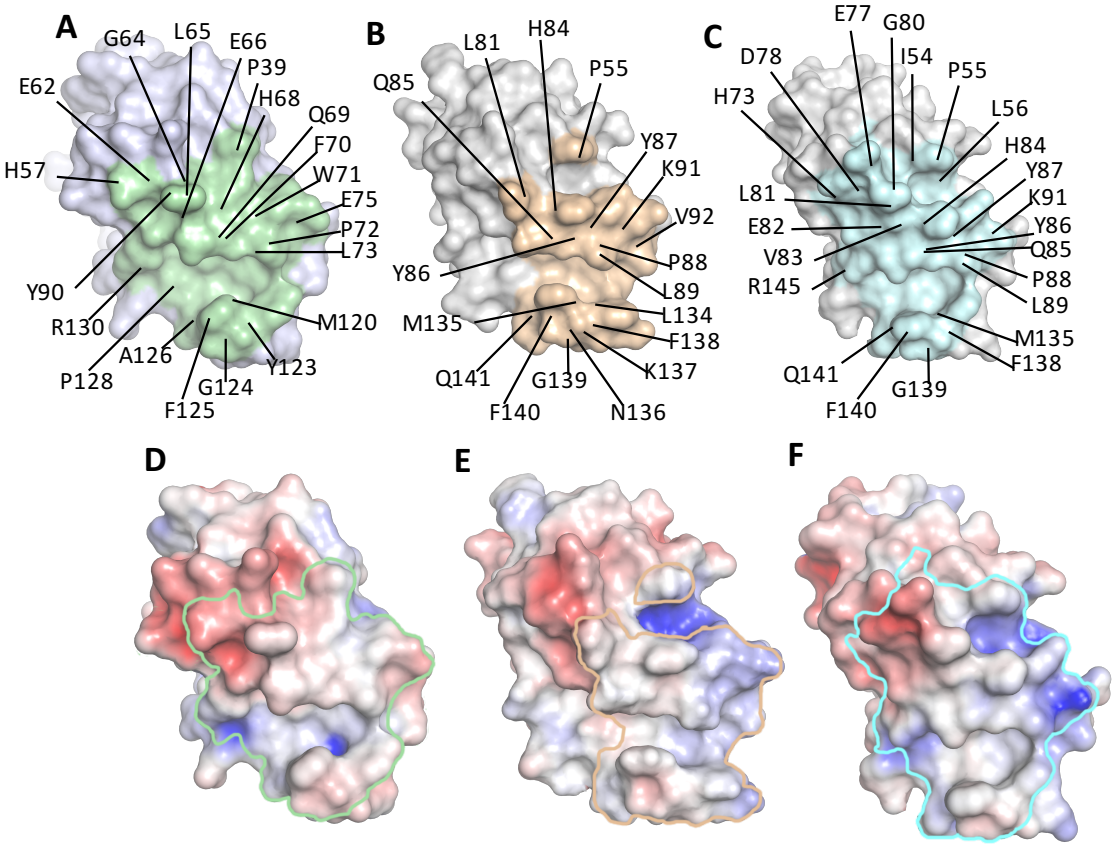

Figure S2: Epitope mapping of FZD mAbs. Molecular outline of the epitope for mAbs A) F2.I on FZD5, B) F7.B on FZD7 and C) F6 on FZD7, with epitope residues labeled. B) Electrostatic rendering for D) FZD5-CRD from the co-complex crystal structure with F2.I Fab, E) FZD7-CRD from the co-complex crystal structure with F7.B Fab and F) FZD7-CRD from the co-complex crystal structure with F6 Fab. Epitope outlines are marked on each surface, with green for mAb F2.I, wheat for mAb F7.B and cyan for mAb F6.

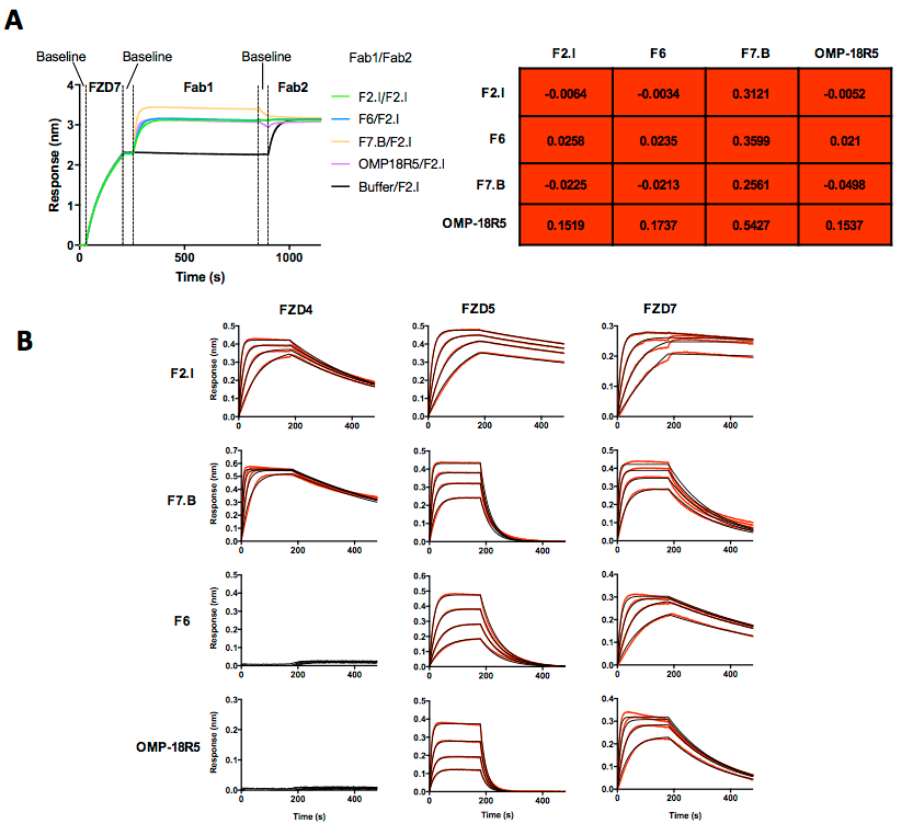

	F2.I	F6	F7.B	OMP-18R5
F2.I	-0.0064	-0.0034	0.3121	-0.0052
F6	0.0258	0.0235	0.3599	0.021
F7.B	-0.0225	-0.0213	0.2561	-0.0498
OMP-18R5	0.1519	0.1737	0.5427	0.1537

Fab	FZD4-CRD			FZD5-CRD			FZD7-CRD		
	k_{on} (1/Ms)	k_{off} (1/s)	K_D (nM)	k_{on} (1/Ms)	k_{off} (1/s)	K_D (nM)	k_{on} (1/Ms)	k_{off} (1/s)	K_D (nM)
F2.I	$5.9\times10^{5} \pm 8.5\times10^{3}$	$26.0\times10^{-4} \pm 1.3\times10^{-5}$	4.5 ± 0.1	$3.4\times10^{5} \pm 2.3\times10^{3}$	$5.7\times10^{-4} \pm 0.4\times10^{-5}$	1.7 ± 0.1	$3.2\times10^{5} \pm 6.8\times10^{3}$	$1.1\times10^{-4} \pm 1.8\times10^{-5}$	0.3 ± 0.1
F7.B	$12.3\times10^{5} \pm 9.0\times10^{3}$	$18.5\times10^{-4} \pm 1.7\times10^{-5}$	1.5 ± 0.1	$6.9\times10^{5} \pm 5.8\times10^{3}$	$283.0\times10^{-4} \pm 40\times10^{-5}$	40.8 ± 0.7	$11.5\times10^{5} \pm 15.3\times10^{3}$	$59.7\times10^{-4} \pm 8.4\times10^{-5}$	5.2 ± 0.2
F6	nb	nb	nb	$2.7\times10^{5} \pm 2.1\times10^{3}$	$154.7\times10^{-4} \pm 23.3\times10^{-5}$	56.6 ± 0.4	$4.0\times10^{5} \pm 2.5\times10^{3}$	$18.0\times10^{-4} \pm 1.5\times10^{-5}$	4.5 ± 0.1
OMP18R5	nb	nb	nb	$4.9\times10^{5} \pm 10.8\times10^{3}$	$520.0\times10^{-4} \pm 112.7\times10^{-5}$	106.3 ± 2.6	$7.6\times10^{5} \pm 13.3\times10^{3}$	$52.0\times10^{-4} \pm 11.3\times10^{-5}$	6.8 ± 0.3

Figure S3: Kinetics of FZD-CRD binding to Fabs using BLI. A) Epitope binning by tandem competition assay using BLI. The left figure shows the raw data where the secondary antibody (F2.I Fab) competes with the various primary antibodies bound to FZD-CRD immobilized on Ni-NTA sensors. The right is a numeric representation of competition and epitope binning, where primary antibodies tested are listed in the left column and secondary competing antibodies are listed at the top. Data indicates the response of competing antibody binding compared to the maximum competing antibody response in the absence of the primary antibody**.** The data indicates that all Fabs compete with each other to bind FZD. B) The represented plots show the binding of FZD-CRD

(FZD4, FZD5 and FZD7) to F2.I, F7.B, F6 and OMP18R5 Fabs. The data (red) was fit using a 1:1 model (black). Values for kinetic parameters (k_{on}, k_{off} and K_D) are listed below. The data represents three independent measurements with mean and standard error of mean (SEM) reported.

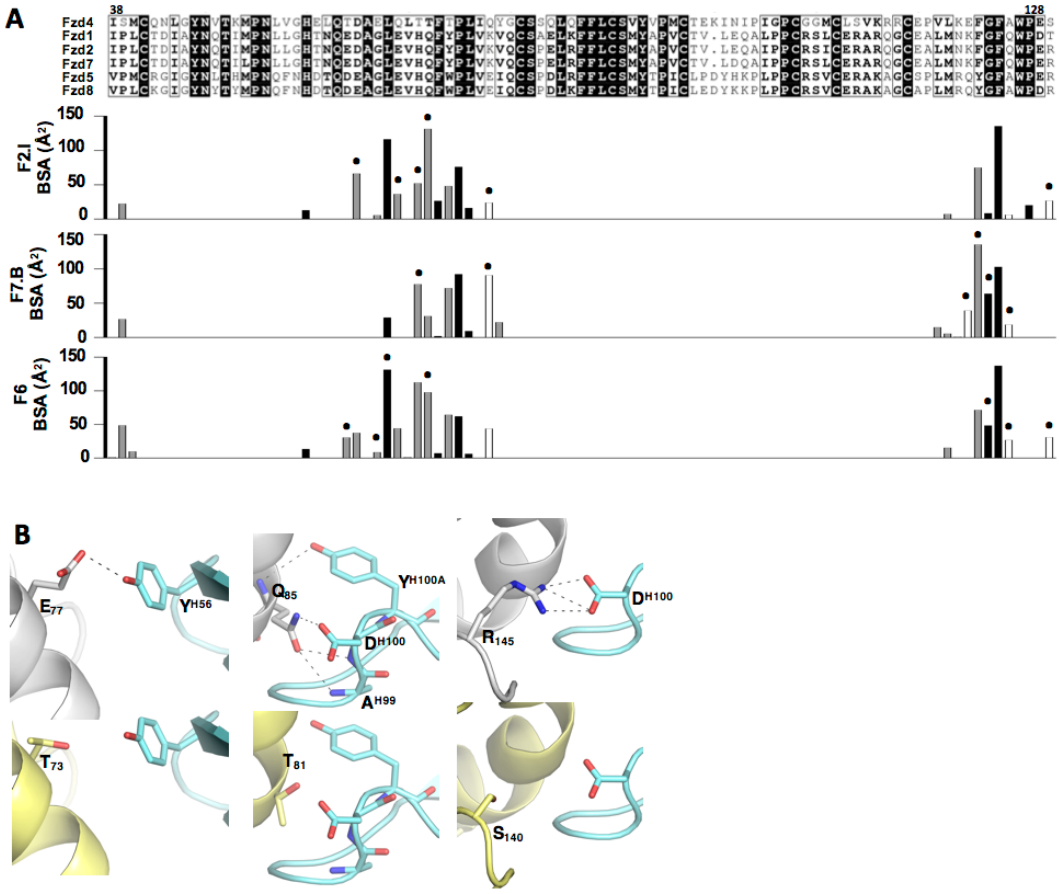

Figure S4: Molecular understanding of multi-specific FZD recognition by mAbs. A) Sequence alignment of FZD CRDs and corresponding interaction plot for mAbs F2.I, F7.B and F6 recognition. The residue numbering for FZD5-CRD is shown at the top. Circles represent residues that form H-bonds. The black, grey and white bars of buried surface area (BSA) derived from the antibody-antigen structures represent residues that are conserved, similar and variant, respectively, between FZD-CRDs. B) Structural differences between the residues of FZD7 (grey, top, crystal structure) and FZD4 (yellow, bottom, model) that limit mAb F6 binding to FZD4.

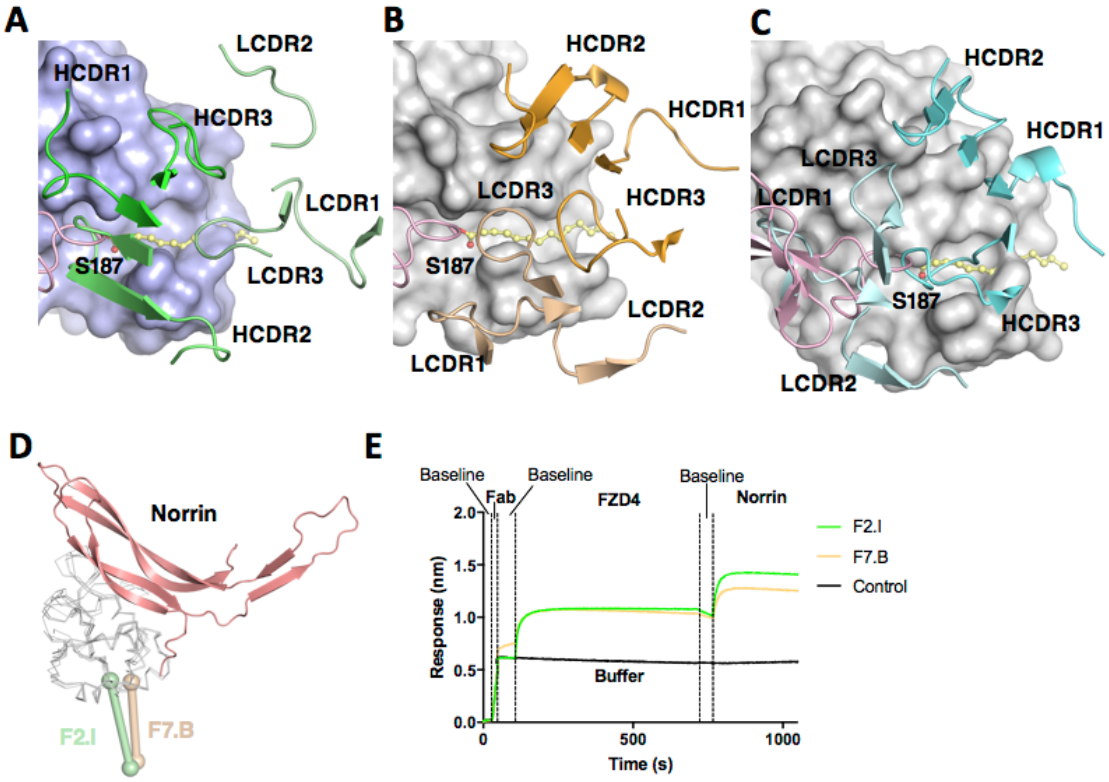

Figure S5: Blocking of Wnt site 1 by mAbs. Blocking of the Wnt (pink) palmitoleic acid (yellow) interaction on FZD by antibody CDRs of mAbs A) F2.I (green), B) F7.B (orange) and C) F6 (cyan). D) The Norrin interaction site on FZD is different from the interaction site of the antibodies. E) BLI competition assay between Fabs and Norrin to bind to FZD4. Norrin is able to bind to FZD4 even in the presence of these Fabs.

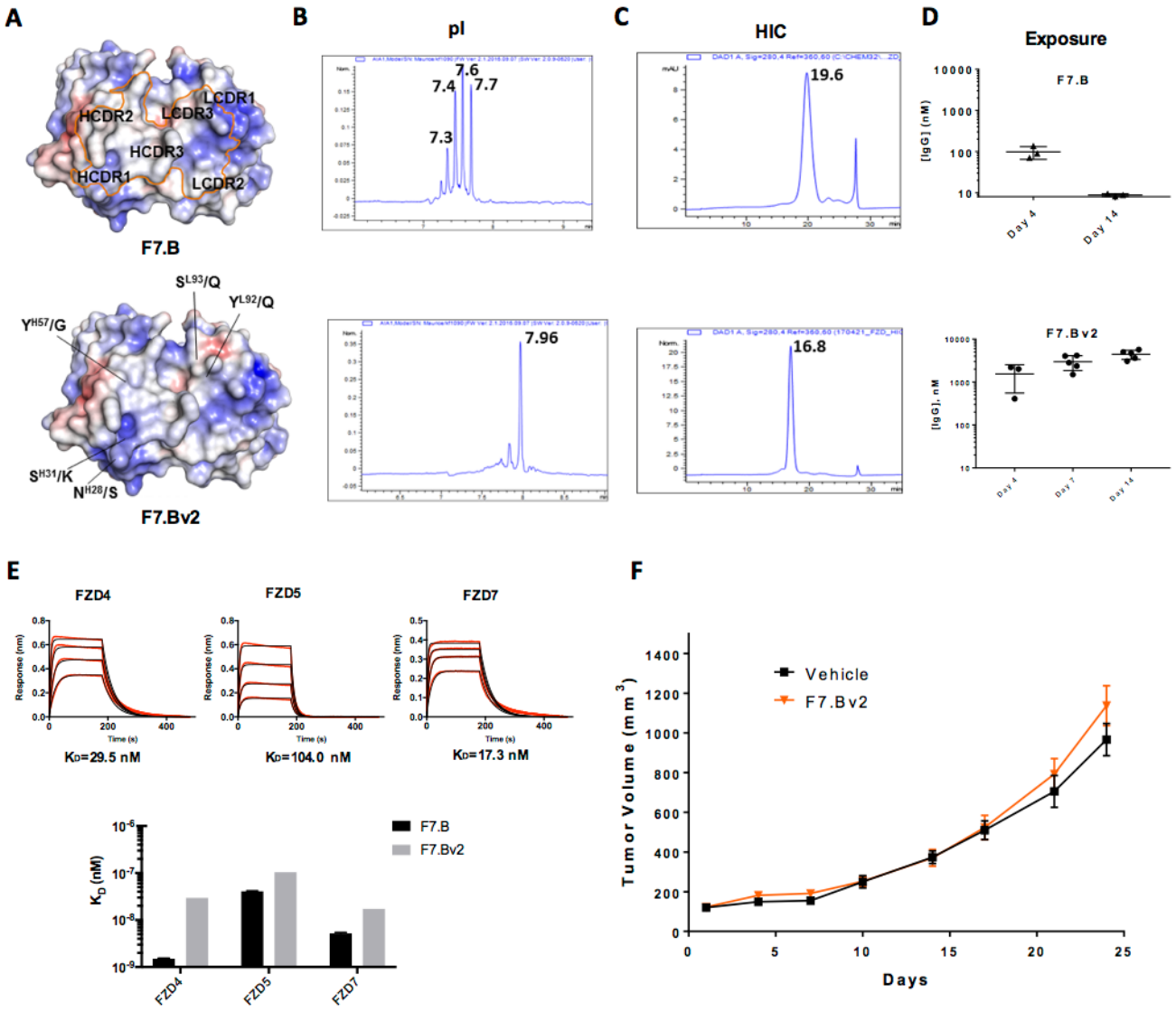

Figure S6: Structure-based engineering of mAb F7.B. A) Electrostatic rendering of F7.B and variant designed to improve hydrophobicity, pI and exposure. B) pI profile of the mAbs measured by isoelectric focusing. C) HIC profile of the mAb F7.B and variant showing retention volumes. D) Exposure profile of mAb F7.B and variant. E) Binding of FZD-CRD (FZD4, FZD5 and FZD7) to F7.Bv2 Fab. The data (red) was fit using a 1:1 model (black). The plot below represents the comparison of K_D's between parent F7.B and variant F7.Bv2. F) HPAF-II xenograft study showing tumor volume for mice treated with vehicle or F7.Bv2 (30 mg/kg), i.p. twice per week (N=12 per group).

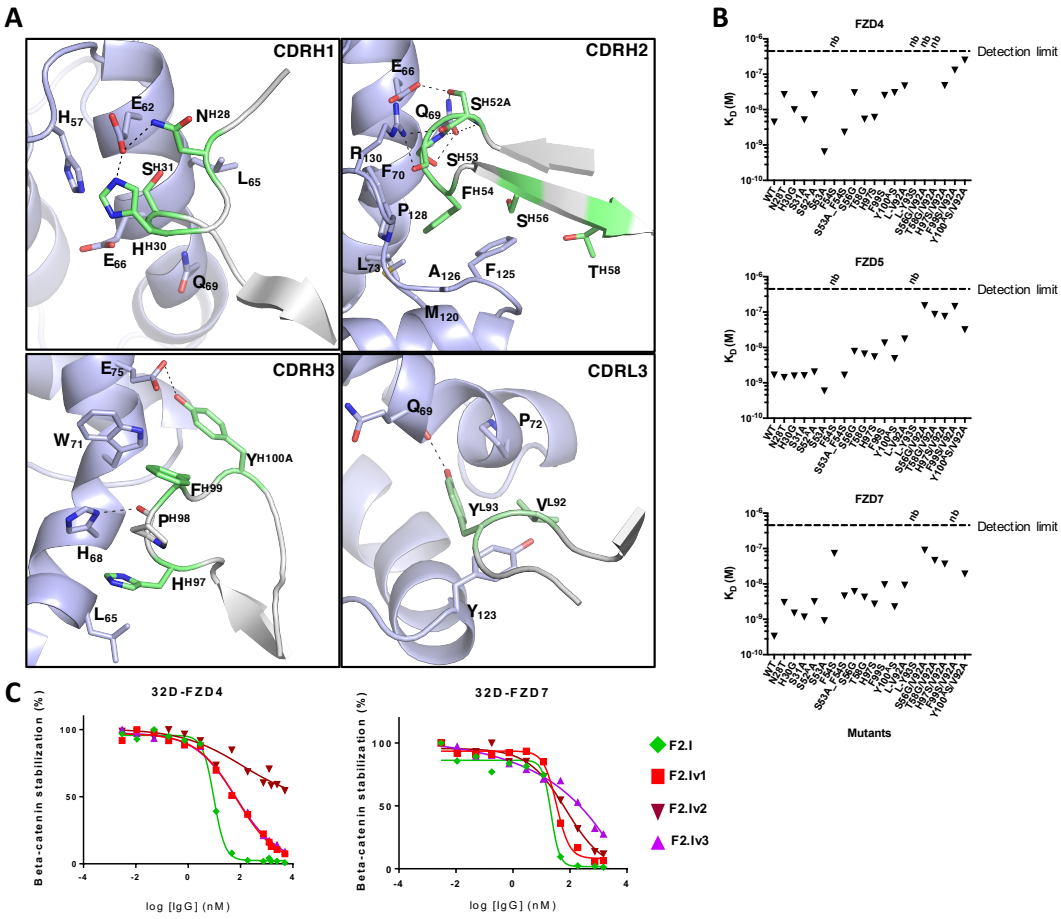

Figure S7: Design, binding and *in vitro* potency of mAb F2.I variants. A) mAb F2.I variants designed to decrease FZD5 binding affinity. CDR residues are shown in grey, while the residues that were mutated are colored green. B) Binding of F2.I Fab variants to FZD-CRDs. nb denotes no detectable binding at the maximum concentration tested. C) β-catenin stabilization assays in 32D-FZD4 and 32D-FZD7 cells for mAb F2.I (green) and its variants, mAbs F2.Iv1 (red), F2.Iv2 (brown), and F2.Iv3 (purple).

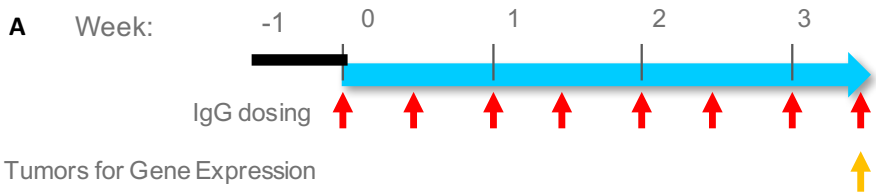

B

Group	n	IgG	mg/kg	Route
1	12	PBS Vehicle	-	IP
2	12	F6	30	IP
3	12	F2.Iv2	30	IP
4	12	OMP-18R5	30	IP

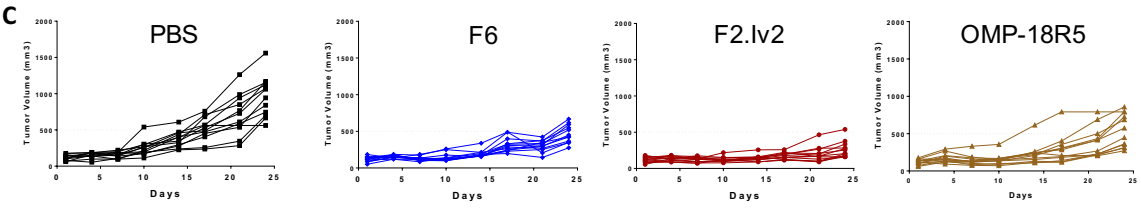

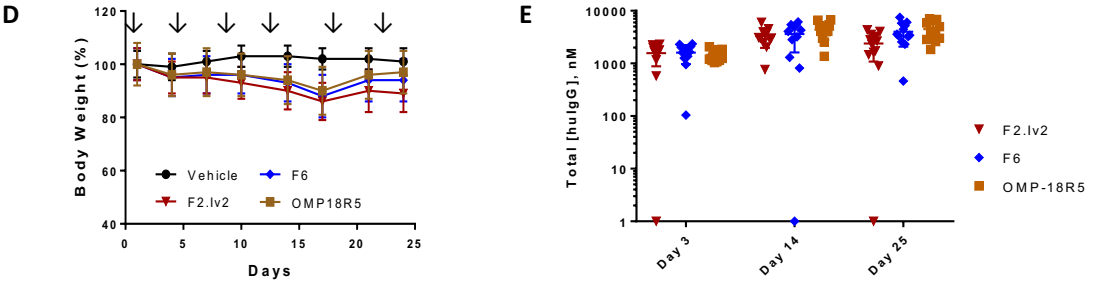

Figure S8: HPAF-II *in vivo* efficacy study design, mouse body weights and mAb plasma exposures. A) *In vivo* study design, depicting when mice were dosed and when tumor samples were collected. B) Summary table of treatment groups. C) Individual spider plots showing tumor volumes for each mouse over the course of the study. D) Percent original body weights of mice treated with Vehicle, mAbs OMP-18R5, F6 or F2.Iv2 over the course of the study. Arrows indicate dosing. *Note: one mAb F2.Iv2-treated mouse (out of 12) was euthanized on day 21 due to body weight loss (included in analysis). E) Plasma antibody exposures in mice treated with Vehicle, mAbs OMP-18R5, F6 or F2.Iv2 over the course of the study. Note: mice with detected Ab less than 1 nM; likely assay error.

Table S1: Data collection and refinement statistics.

	F2.I Fab-FZD5-CRD	F7.B Fab-FZD7-CRD	F6 Fab-FZD7-CRD
Wavelength (Å)	0.97949	0.97949	1.03327
Resolution range (Å)	35.87 - 1.80 (1.86 - 1.80)	37.24 - 2.10 (2.18 - 2.10)	29.74 - 2.50 (2.59 - 2.50)
Space group	P 6_1 2 2	P 2_1 2_1 2_1	C 2
Cell dimensions			
a, b, c (Å)	101.4 101.4 196.5	41.5 103.4 144.2	139.6 85.8 104.1
α, β, γ (°)	90 90 120	90 90 90	90 95.82 90
Total reflections	1,212,944 (120,611)	270,616 (27,186)	138,484 (14,922)
Unique reflections	56,002 (5,489)	37,237 (3,674)	41,997 (4,241)
Multiplicity	21.7 (22.0)	7.3 (7.4)	3.3 (3.5)
Completeness (%)	100 (100)	99.9 (99.9)	98.7 (99.8)
Mean I/sigma(I)	25.1 (1.9)	12.6 (2.0)	7.5 (1.5)
Wilson B-factor (Å^2)	31.7	33.2	36.8
R_{merge}	0.085 (1.963)	0.124 (1.120)	0.196 (1.011)
R_{pim}	0.019 (0.426)	0.049 (0.438)	0.128 (0.627)
$CC_{1/2}$	1.000 (0.699)	0.998 (0.701)	0.975 (0.659)
Refinement Statistics			
Reflections used in refinement	55,998 (5,489)	37,226 (3,673)	41,964 (4,235)
Reflections used for R_{free}	2,000 (196)	1,862 (184)	1,998 (202)
R_{work} / R_{free}	0.19/0.23	0.19/0.24	0.23/0.28
Number of non-hydrogen atoms	4,734	4,582	8,637
Macromolecules	4,278	4,207	8,416
Hetero	70	67	58
Solvent	386	308	163
RMS(bonds) (Å)	0.006	0.007	0.002
RMS(angles) (°)	0.90	0.92	0.52
Ramachandran favored (%)	97.8	97.4	96.5
Ramachandran allowed (%)	2.2	2.6	3.3
Average B-factor (Å^2)	37.0	39.6	41.8
Macromolecules	36.5	39.3	41.7
Hetero	47.7	59.4	61.8
Solvent	40.7	39.2	37.4

* Values in parentheses refer to the highest resolution bin.

Table S2: Interactions for the F2.I Fab-FZD5-CRD complex.

FZD5-CRD residue (BSA Å^2)	Interaction Type	F2.I residues
Pro39 (22.57)		
Pro	VDW	H-Pro98
His57 (12.98)		
His	VDW	H-His30, H-Ser31
Glu62 (66.40)		
Glu^{OE1}	HB	H-Asn28^{ND2}
Glu^{OE1}	SB	H-His30^{NE2}
Glu	VDW	H-Asn28, H-His30, H-Ser31
Gly64 (5.72)		
Gly64	VDW	H-His97
Leu65 (116.45)		
Leu65	VDW	H-Phe27, H-Asn28, H-Ser31, H-Ser32, H-Arg94, H-His97
Glu66 (37.58)		
Glu^{OE1}	HB	H-Ser52A^{OG}
Glu	VDW	H-His30, H-Ser31, H-Ser52A, H-Ser53
His68 (52.24)		
His^{ND1}	HB	H-Pro98^{O}
His	VDW	H-Tyr95, H-His97, H-Pro98, H-Phe99
Gln69 (131.48)		
Gln69^{NE2}	HB	H-Ser31^{O},
Gln69^{OE1}	HB	H-Ser52A^{N}, H-Ser53^{N}, H-Ser53^{OG}
Gln69^{O}	HB	L-Tyr93^{OH}
Gln69	VDW	H-Ser31, H-Ser32, H-Ser33, H-Tyr52, H-Ser52A, H-Ser53, H-Phe54, H-Tyr95, L-Tyr93
Phe70 (26.64)		
Phe70	VDW	H-Ser53, H-Phe54, L-Tyr93
Trp71 (48.20)		
Trp71	VDW	H-Pro98, H-Phe99, H-Tyr100A, L-Tyr93
Pro72 (76.21)		
Pro72	VDW	H-Tyr95, H-Phe99, H-Tyr100A, L-Val92, L-Tyr93
Leu73 (16.27)		
Leu73	VDW	H-Phe54, L-Tyr93

Glu75 (24.07)		
Glu^{OE1}	HB	H-Tyr100A^{OH}
Glu	VDW	H-Tyr100A
Tyr90 (0.25)		
Tyr90	VDW	H-Ser53
Met120 (7.37)		
Met120	VDW	H-Phe54
Tyr123 (75.09)		
Tyr123	VDW	L-Val92, L-Tyr93, L-Leu94
Gly124 (8.57)		
Gly	VDW	H-Thr58
Phe125(135.58)		
Phe	VDW	H-Tyr52, H-Phe54, H-Ser56, H-Thr58, L-Tyr93, L-Leu94
Ala126 (6.37)		
Ala	VDW	H-Phe54
Pro128 (20.26)		
Pro	VDW	H-Ser53, H-Phe54
Arg130 (26.90)		
Arg^{NH1}	HB	H-Ser52A^{O}
Arg	VDW	H-Ser52A, H-Ser53, H-Phe54, H-Gly55

Table S3: Interactions for the F7.B Fab-FZD7-CRD complex.

FZD7-CRD residue (BSA Å^2)	Interaction Type	F7.B residues
Pro55 (26.81)		
Pro	VDW	H-Tyr56
Leu81 (29.08)		
Leu	VDW	H-Tyr58
His84 (77.65)		
His^{NE2}	HB	H-Tyr50^{OH}
His	VDW	H-Tyr50, H-Tyr52, H-Tyr56, H-Tyr58
Gln85 (31.16)		
Gln	VDW	H-Trp100
Phe86 (1.98)		
Phe	VDW	H-Trp100
Tyr87 (71.94)		
Tyr	VDW	H-Tyr52, H-Tyr-54, H-Tyr56
Pro88 (92.30)		
Pro	VDW	H-Tyr52, H-Phe97, H-Tyr98, H-Thr99, H-Trp100
Leu89 (9.40)		
Leu	VDW	H-Phe97, H-Trp100
Lys91 (90.73)		
Lys^{NZ}	HB	H-Tyr98^{OH}
Lys	VDW	H-Ser30, H-Ser31, H-Tyr54, H-Tyr98
Val92 (22.24)		
Val	VDW	H-Phe97, H-Tyr98
Leu134 (14.89)		
Leu	VDW	H-Phe97, H-Trp100
Met135 (5.55)		
Met135	VDW	H-Trp100
Asn136 (0.98)		
Asn	VDW	L-Ser50
Lys137 (39.21)		
Lys^{O}	HB	L-Ser50^{OG}
Lys	VDW	L-Tyr49, L-Ser50, L-Ser53

Phe138 (135.58)		
Phe^{O}	HB	L-Tyr91^{OH}
Phe	VDW	H-Tyr96, H-Phe97, H-Trp100, H-Gly100A, L-Ser31, L-Ala32, L-Tyr49, L-Ser50, L-Tyr91
Gly139 (63.86)		
Gly^{N}	HB	L-Ser50^{OG}
Gly^{O}	HB	L-Ser31^{N}, L-Ala32^{N}
Gly	VDW	L-Ser30, L-Ser31, L-Ala32, L-Ser50, L-Tyr91
Phe140 (102.94)		
Phe140	VDW	H-Trp100, L-Ser30, L-Ala32, L-Tyr91, L-Tyr92
Gln141 (18.68)		
Gln141^{N}	HB	L-Ser30^{OG}
Gln	VDW	L-Ser30

Table S4: Interactions for the F6 Fab-FZD7-CRD complex.

FZD7-CRD residue (BSA Å^2)	Interaction Type	F6 residues
Ile54 (1.17)		
Ile	VDW	H-Tyr54
Pro55 (48.68)		
Pro	VDW	H-Ser53, H-Tyr54
Leu56 (9.96)		
Leu	VDW	H-Tyr54
His73 (13.52)		
His	VDW	L-Tyr93
Glu77 (30.66)		
Glu^{OE1}	HB	H-Tyr56^{OH}
Glu	VDW	H-Tyr56^{OH}
Asp78 (37.55)		
Asp	VDW	L-Tyr93
Gly80 (8.70)		
Gly^{O}	HB	H-Tyr54^{OH}
Gly	VDW	H-Tyr54
Leu81 (131.53)		
Leu^{N}	HB	H-Tyr54^{OH}
Leu	VDW	H-Tyr52, H-Tyr54, H-Tyr56, H-Tyr100A, L-Trp91, L-Tyr93, L-Gly94
Glu82 (44.21)		
Glu	VDW	H-Asp100, H-Tyr100A, L-Trp91, L-Tyr93
Val83 (1.34)		
Val	VDW	H-Tyr54
His84 (112.60)		
His	VDW	H-Tyr30, H-Tyr31, H-Tyr32, H-Ser33, H-Tyr52, H-Ser52A, H-Ser53, H-Tyr54, H-Tyr100A
Gln85 (97.88)		
Gln^{OE1}	HB	H-Ala99^{N}, H-Asp100^{N}
Gln^{NE1}	HB	H-Asp100^{OD2}
Gln^{N}	HB	H-Tyr100A^{OH}

Gln	VDW	H-Ser96, H-Pro97, H-Gly98, H-Ala99, H-Asp100, H-Tyr100A
Phe86 (7.23)		
Phe	VDW	H-Pro97, H-Gly98
Tyr87 (64.49)		
Tyr	VDW	H-Tyr30, H-Tyr31, H-Ser53
Pro88 (62.15)		
Pro	VDW	H-Tyr31, H-Tyr32, H-Pro97
Leu89 (6.36)		
Leu	VDW	H-Pro97
Lys91 (43.84)		
Lys	VDW	H-Tyr31
Met135 (15.40)		
Met	VDW	H-Pro97, H-Gly98
Phe138 (71.61)		
Phe	VDW	H-Tyr32, H-Arg94, H-Ser96, H-Pro97, H-Asp101, L-Tyr55
Gly139 (48.49)		
Gly^{O}	HB	L-Ser56^{N}
Gly	VDW	L-Tyr49, L-Tyr55, L-Ser56
Phe140 (137.25)		
Phe	VDW	H-Ser96, H-Pro97, H-Gly98, H-Ala99, H-Asp101, L-Leu46, L-Tyr49, L-Tyr55
Gln141 (26.90)		
Gln^{N}	HB	L-Tyr49^{OH}
Gln	VDW	H-Gly98, L-Tyr49
Arg145 (31.02)		
Arg^{NH1}	SB	H-Asp100^{OD1}, H-Asp100^{OD2}
Arg^{NH2}	SB	H-Asp100^{OD1}
Arg	VDW	H-Asp100

Table S5: Binding affinities for F2.I Fab variants to FZD-CRDs.

	FZD4-CRD	FZD5-CRD	FZD7-CRD
Fab	**K_D (nM)**	**K_D (nM)**	**K_D (nM)**
F2.I	4.5	1.7	0.3
N28T	27	1.4	3.0
H30G	9.9	1.6	1.5
S31A	5.1	1.6	1.2
S52^{A}A	27	2.0	3.2
S53A	0.6	0.6	0.9
F54S	No binding	Poor Binding	72.3
S53A_F54S	2.3	1.7	4.6
S56G	30	7.7	6.1
T58G	5.4	6.5	4.2
H97S	6.0	5.4	2.7
F99S	25.0	13.0	9.5
Y100^{A}S	30.0	4.8	2.3
L-V92A	46.8	17.4	9.0
L-Y93S	No binding	No binding	No binding
S56G/L-V92A	Poor Binding	151.0	89.4
T58G/L-V92A	Poor Binding	86.0	46.0
H97S/L-V92A	47.7	75.5	36.2
F99S/L-V92A	130.0	144.0	Poor Binding
Y100^{A}S/L-V92A	250.7	31.7	19.0

*L- indicates light chain mutations

Table S6: Binding kinetics for F2.I Fab lead variants to different FZD-CRDs.

Antibody	FZD1			FZD2			FZD4			FZD5			FZD7			FZD8		
	k_{on} (1/Ms)	k_{off} (1/s)	K_D (nM)	k_{on} (1/Ms)	k_{off} (1/s)	K_D (nM)	k_{on} (1/Ms)	k_{off} (1/s)	K_D (nM)	k_{on} (1/Ms)	k_{off} (1/s)	K_D (nM)	k_{on} (1/Ms)	k_{off} (1/s)	K_D (nM)	k_{on} (1/Ms)	k_{off} (1/s)	K_D (nM)
F2.I	$2.3\times10^{5} \pm 8.1\times10^{3}$	$4.0\times10^{-4} \pm 3.0\times10^{-5}$	1.8 ± 0.2	$2.2\times10^{5} \pm 1.8\times10^{3}$	$3.0\times10^{-4} \pm 5.0\times10^{-5}$	1.3 ± 0.2	$5.9\times10^{5} \pm 8.5\times10^{3}$	$26.0\times10^{-4} \pm 1.3\times10^{-5}$	4.5 ± 0.1	$3.4\times10^{5} \pm 2.3\times10^{3}$	$5.7\times10^{-4} \pm 0.4\times10^{-5}$	1.7 ± 0.1	$3.2\times10^{5} \pm 6.8\times10^{3}$	$1.1\times10^{-4} \pm 1.8\times10^{-5}$	0.3 ± 0.1	$3.3\times10^{5} \pm 9.5\times10^{3}$	$12.0\times10^{-4} \pm 7.0\times10^{-5}$	3.5 ± 0.3
F2.Iv1	$0.9\times10^{5} \pm 2.6\times10^{3}$	$12.4\times10^{-4} \pm 6.2\times10^{-5}$	13.2 ± 0.7	$0.9\times10^{5} \pm 0.2\times10^{3}$	$6.5\times10^{-4} \pm 6.3\times10^{-5}$	7.0 ± 0.7	$3.8\times10^{5} \pm 12.0\times10^{3}$	$176.0\times10^{-4} \pm 47.2\times10^{-5}$	46.8 ± 0.5	$2.2\times10^{5} \pm 11.7\times10^{3}$	$38.3\times10^{-4} \pm 5.8\times10^{-5}$	17.4 ± 0.7	$1.2\times10^{5} \pm 6.0\times10^{3}$	$10.5\times10^{-4} \pm 5.2\times10^{-5}$	9.0 ± 0.9	$1.8\times10^{5} \pm 7.0\times10^{3}$	$67.3\times10^{-4} \pm 3.0\times10^{-5}$	38.0 ± 1.7
F2.Iv2	$0.7\times10^{5} \pm 1.0\times10^{3}$	$18.7\times10^{-4} \pm 10.7\times10^{-5}$	28.0 ± 1.6	$0.7\times10^{5} \pm 0.4\times10^{3}$	$10.4\times10^{-4} \pm 8.0\times10^{-5}$	15.5 ± 1.3	$2.9\times10^{5} \pm 10.8\times10^{3}$	$722.0\times10^{-4} \pm 520.4\times10^{-5}$	250.7 ± 25.0	$1.7\times10^{5} \pm 3.8\times10^{3}$	$53.3\times10^{-4} \pm 9.3\times10^{-5}$	31.7 ± 1.2	$0.8\times10^{5} \pm 5.0\times10^{3}$	$15.7\times10^{-4} \pm 0.3\times10^{-5}$	19.0 ± 1.2	$1.4\times10^{5} \pm 4.0\times10^{3}$	$109.7\times10^{-4} \pm 8.8\times10^{-5}$	75.6 ± 1.6
F2.Iv3	$0.8\times10^{5} \pm 1.1\times10^{3}$	$46.0\times10^{-4} \pm 13.9\times10^{-5}$	57.8 ± 0.9	$0.9\times10^{5} \pm 2.8\times10^{3}$	$22.2\times10^{-4} \pm 11.2\times10^{-5}$	23.8 ± 0.4	$3.5\times10^{5} \pm 5.4\times10^{3}$	$167.7\times10^{-4} \pm 16.7\times10^{-5}$	47.7 ± 0.5	$2.3\times10^{5} \pm 11.2\times10^{3}$	$175.7\times10^{-4} \pm 44.8\times10^{-5}$	75.5 ± 2.2	$1.0\times10^{5} \pm 5.4\times10^{3}$	$36.6\times10^{-4} \pm 4.2\times10^{-5}$	36.2 ± 2.4	$1.8\times10^{5} \pm 0.7\times10^{3}$	$196.3\times10^{-4} \pm 23.3\times10^{-5}$	107.0 ± 1.7

Table S7. *In vitro* properties of mAb F2.I variants.

Antibody	Inhibition of β-catenin stabilization (IC_{50} (nM)/ max % inhibition)						Binding affinity [K_D (nM)] *						HPAF proliferation inhibition (IC_{50} (nM)/ max % inhibition)
	FZD1	FZD2	FZD4	FZD5	FZD7	FZD8	FZD1	FZD2	FZD4	FZD5	FZD7	FZD8	
F2.I	0.98 / 98	1.7 / 99	9.6 / 99	8.5 / 96	21.8 / 99	0.12 / 99	1.8 ± 0.2	1.3 ± 0.2	4.5 ± 0.1	1.7 ± 0.1	0.30 ± 0.05	3.5 ± 0.3	3.3 / 94
F2.Iv1	4.0 / 92	3.5/ 90	69.5 / 93	13.8 / 82	33.8 / 94	1.2 / 95	13.2 ± 0.7	7.0 ± 0.7	46.8 ± 0.5	17.4 ± 0.7	9.0 ± 0.9	38.0 ± 1.7	63.9 / 96
F2.Iv2	7.6 / 87	7.3 / 90	114.4 / 45	15.7 / 66	72.8 / 88	6.8 / 86	28.0 ± 1.6	15.5 ± 1.3	251 ± 25	31.7 ± 1.2	19.0 ± 1.2	75.6 ± 1.6	69.9 / 82
F2.Iv3	11.0 / 87	4.1 / 87	67.1 / 91	13.3 / 39	212.3 / 73	7.9 / 76	57.8 ± 0.9	23.8 ± 0.4	47.7 ± 0.5	75.5 ± 2.2	36.2 ± 2.4	107.0 ± 1.7	327.1 / 66

* The data represents three independent measurements with mean and standard error of mean (SEM) reported.

References:

1. Pavlovic Z, et al. (2018) A synthetic anti-Frizzled antibody engineered for broadened specificity exhibits enhanced anti-tumor properties. *MAbs* 10(8):1157-1167.

2. Chang TH, et al. (2015) Structure and functional properties of norrin mimic wnt for signalling with Frizzled4, Lrp5/6, and proteoglycan. *Elife* 4:e06554.

3. Aricescu AR, Lu W, Jones EY (2006) A time- and cost-efficient system for high-level protein production in mammalian cells. *Acta Crystallogr D Biol Crystallogr* 62(Pt 10):1243–1250.

4. Kabsch W (2010) Xds. *Acta Crystallogr Sect D Biol Crystallogr* 66(2):125–132.

5. McCoy AJ, et al. (2007) Phaser crystallographic software. *J Appl Crystallogr* 40(4):658–674.

6. Janda CY, Waghray D, Levin AM, Thomas C, Garcia KC (2012) Structural basis of Wnt recognition by Frizzled. *Science* 337(6090):59–64.

7. Emsley P, Lohkamp B, Scott WG, Cowtan K (2010) Features and development of Coot. *Acta Crystallogr Sect D Biol Crystallogr* 66(4):486–501.

8. Adams PD, et al. (2010) PHENIX: A comprehensive Python-based system for macromolecular structure solution. *Acta Crystallogr Sect D Biol Crystallogr* 66(2):213–221.

9. Morin A, et al. (2013) Collaboration gets the most out of software. *Elife* 2:e01456.